Manuscript number: JASN-2020-04-0523

SUPPLEMENTARY INFORMATION

Only hyperuricemia with crystalluria but not asymptomatic hyperuricemia drives chronic kidney disease

Markus Sellmayr, Moritz Roman Hernandez Petzsche, Qiuyue Ma, Nils Krüger, Helen Liapis, Andreas Brink, Barbara Lenz, Maria Lucia Angelotti, Viviane Gnemmi, Christoph Kuppe, Hyojin Kim, Eric M.J. Bindels, Ferenc Tajti, Julio Saez-Rodriguez, Maciej Lech, Rafael Kramann, Paola Romagnani, Hans-Joachim Anders, Stefanie Steiger

Table of content

1. Supplementary Methods 2
    1.1 Human microarray gene expression data of different CKD entities 2
2. Supplementary Figures 3
    2.1 Supplementary Figure 1 3
    2.2 Supplementary Figure 2 5
    2.3 Supplementary Figure 3 6
    2.4 Supplementary Figure 4 8
3. Supplementary Movies 10
    3.1 Supplementary Movie 1 10
    3.2 Supplementary Movie 2 10
4. Supplementary Tables 11
    4.1 Supplementary Table 1. Murine primer sequences 11
5. References 12

1. Supplementary Methods

1.1 Human microarray gene expression data of different chronic kidney disease entities

We searched in Nephroseq (www.nephroseq.org) and Gene Expression Omnibus (GEO) [3, 4], and identified five studies – GSE20602 [5], GSE32591 [6], GSE37460 [6], GSE47183 [7, 8], GSE50469 [9] – with human microarray gene expression data for different CKD entities: lupus nephritis (LN), rapidly progressive glomerulonephritis (RPGN), membranous glomerulonephritis (MGN), IgA nephropathy (IgAN), hypertensive nephropathy (HN), diabetic nephropathy (DN), focal segmental glomerulosclerosis (FSGS), and minimal change disease (MCD), as well as healthy tissue from kidney tumor nephrectomy (TN) as control, as previously described [10]. In one dataset, patients were labeled as an overlap of FSGS and MCD (FSGS-MCD). The data were imported in R (R version 3.3.2), processed and normalized involving quality controls [10]. Heatmaps were generated to demonstrate the normalized expression of the inflammatory genes of interest across all CKD entities and the hierarchical clustering of the arrays based on the gene expression Spearman's correlation coefficients.

2. Supplementary Figures

2.1 Supplementary Figure 1

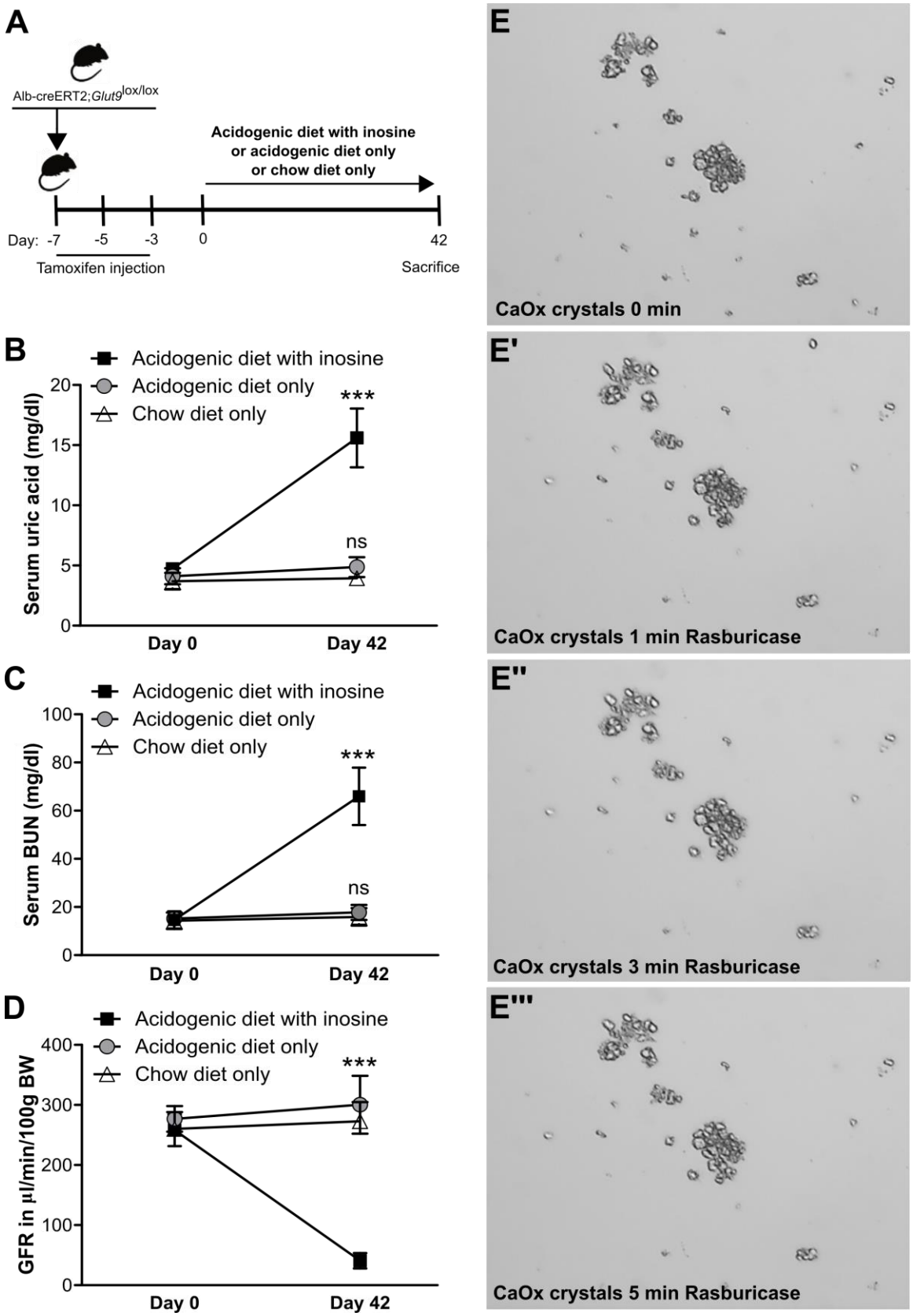

Supplementary Figure 1. Only an acidogenic diet with inosine causes impairment in kidney function but not acidogenic and chow diet without inosine. (**A** - **D**) Alb-creERT2;*Glut9*$^{lox/lox}$ mice were injected with tamoxifen and then placed either on an acidogenic diet with inosine, an acidogenic diet only or standard chow diet only for up to 42 day (**A**). Serum uric acid (**B**), blood urea nitrogen (BUN) (**C**) and GFR (**D**) were measured on day 0 and 42 (n = 5 mice per group). (**E** – **E'''**) Urinary calcium oxalate (CaOx) crystals from mice with chronic oxalate nephropathy did not dissolve upon rasburicase treatment after 5 minutes. Magnification: x400. Data are mean ± SD. *** $p<0.001$; ns, not significant by one-way ANOVA.

81 **2.2 Supplementary Figure 2**

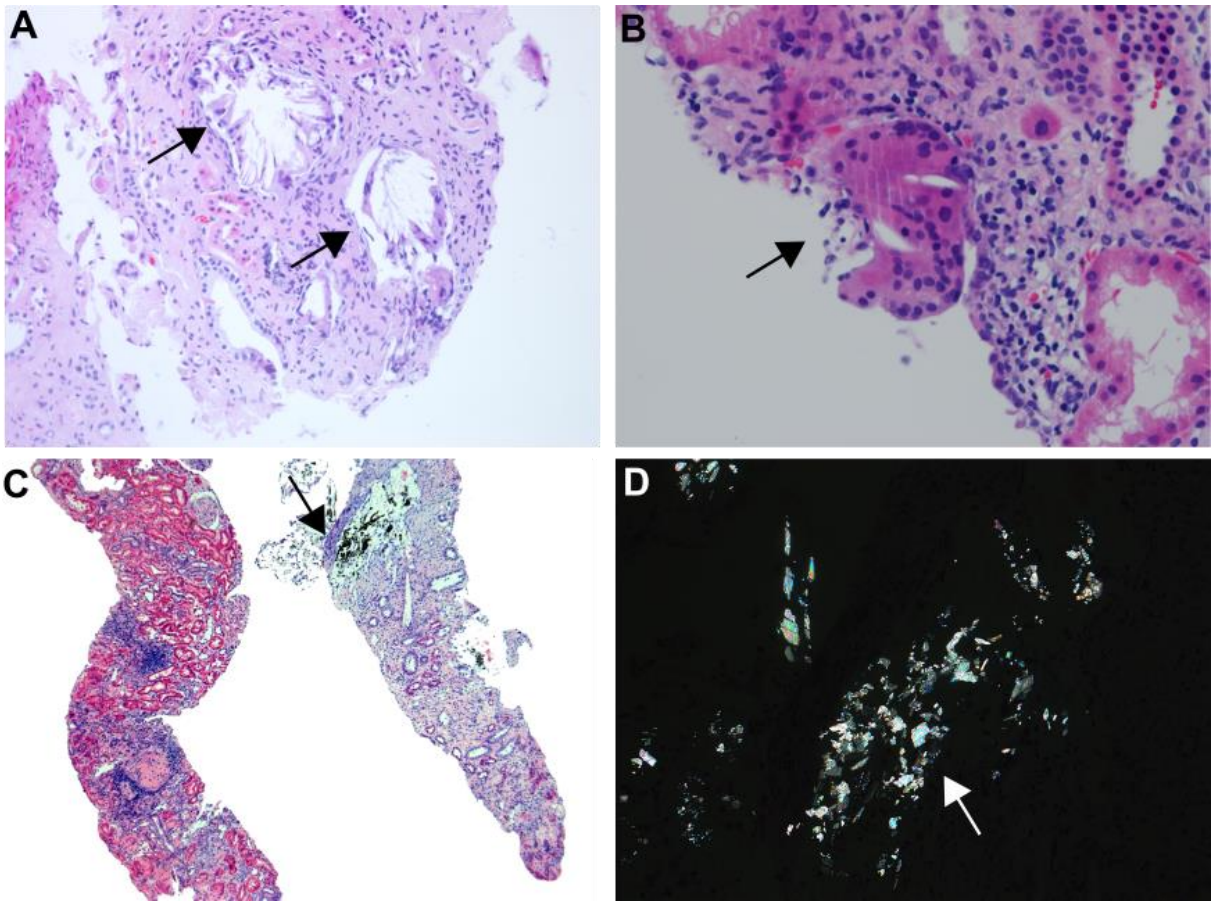

82

83 **Supplementary Figure 2. Histopathological abnormalities on kidney biopsies from patients**
84 **with uric acid crystal deposits.** (**A**) Kidney biopsy shows epithelioid granulomas with colorless
85 ghost-like UA crystals (black arrows, magnification: x100). The patient was a 75 years-old man
86 with CKD, creatinine 3.8 mg/dl and proteinuria 1.6 g/24 hours. (**B**) UA granuloma with spindle
87 shaped UA crystals including giant cell formation containing more than 30 nuclei (black arrow)
88 (PAS stain, magnification: x200). (**C**) Low power of kidney biopsy containing both cortex and
89 medulla shows diffuse interstitial fibrosis and focal glomerulosclerosis in the cortex, and
90 undissolved crystal deposits (black arrow) in the medulla. The patient was a 47 years-old man
91 with a history of biopsy proven IgA nephropathy, now presenting with proteinuria 2 g/24
92 hours (Trichrome stain, magnification: x40). (**D**) UA crystal deposits visualized under a
93 polarizable light microscope (white arrow, same biopsy as in C).

94

95

96

2.3 Supplementary Figure 3

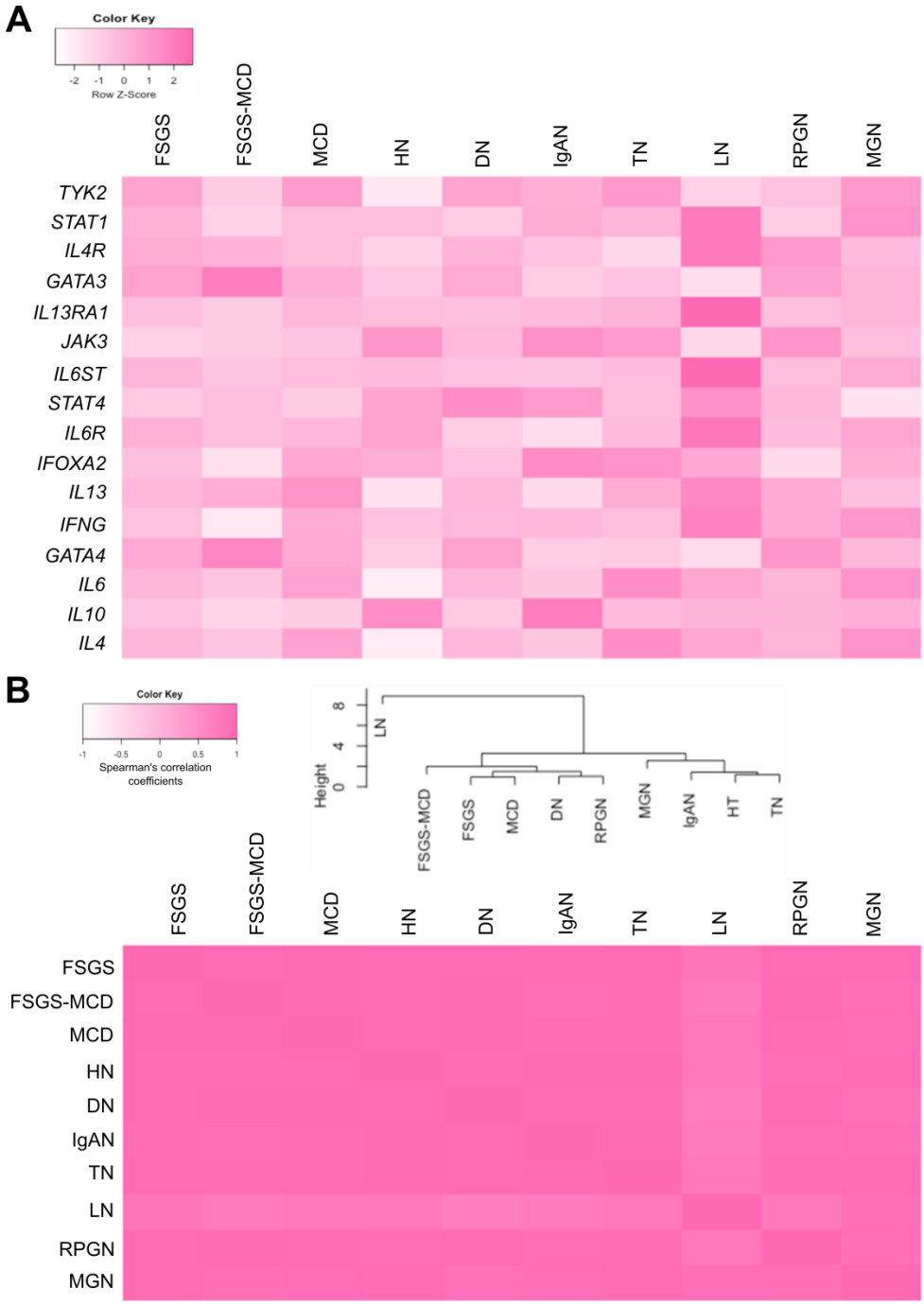

104 **Supplementary Figure 3.** (**A** and **B**) Public available Affymetrix Human Genome arrays
105 predicting gene expression profiles from different human CKD disease entities [10]: lupus
106 nephritis (LN), rapidly progressive glomerulonephritis (RPGN), membranous
107 glomerulonephritis (MGN), IgA nephropathy (IgAN), hypertensive nephropathy (HN), diabetic
108 nephropathy (DN), focal segmental glomerulosclerosis (FSGS), minimal change disease (MCD),
109 and one dataset of patients were labeled as overlap of FSGS-MCD, and healthy tissue from
110 tumor nephrectomy (TN) as control. (**A**) Normalized gene expression of inflammatory genes
111 of CKD entities illustrated as heat map. (**B**) Hierarchical clustering of CKD entities based on the
112 expression of the gene set of interest using the Spearman's correlation coefficient illustrated
113 as heat map.

114

115

116

117

118

119

120

121

122

123

124

125

126

127

128

2.4 Supplementary Figure 4

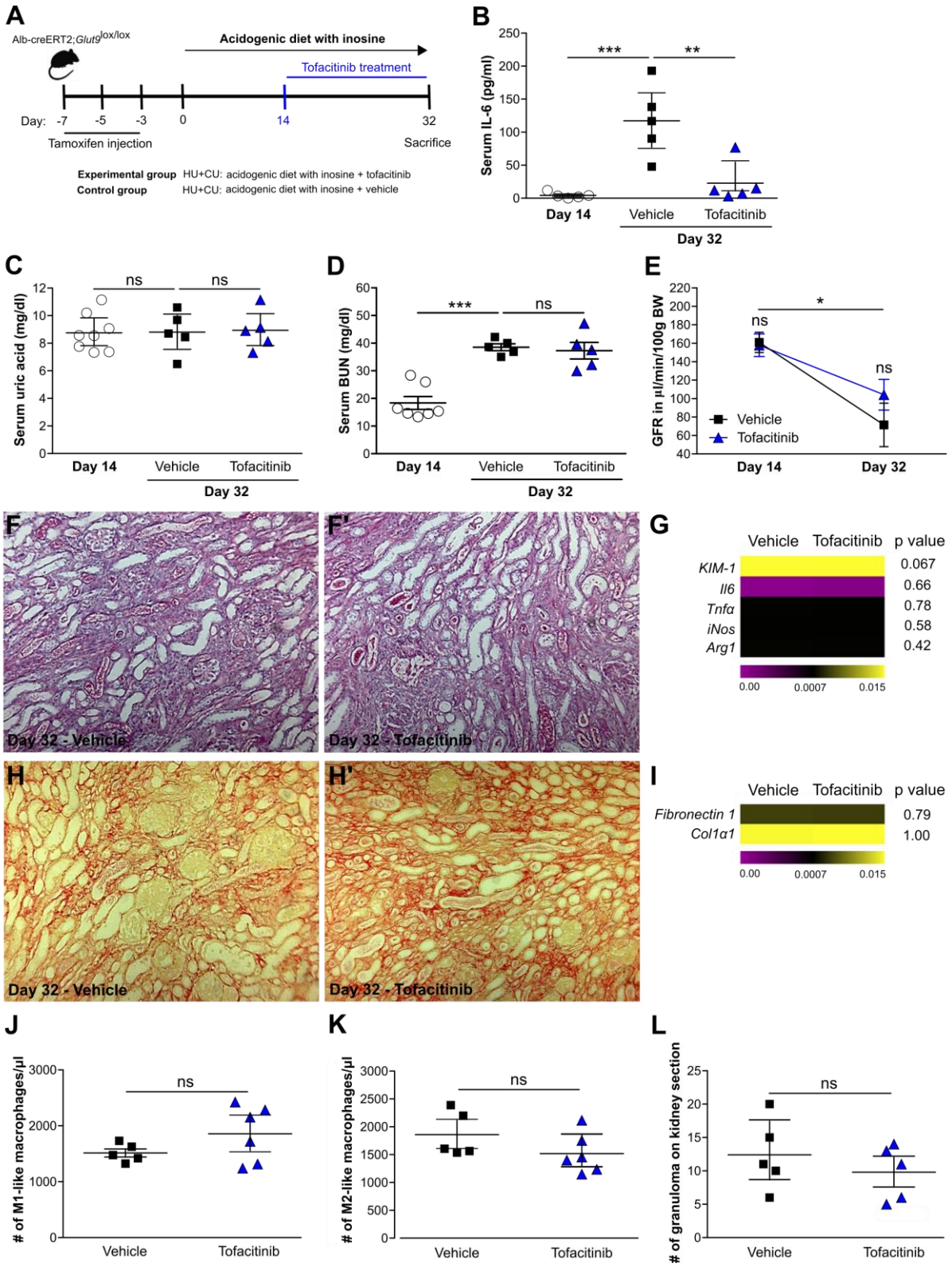

133 **Supplementary Figure 4. Tofacitinib therapy does not prevent crystalluria, granuloma**
134 **formation and CKD progression.** (**A**) Schematic of experimental set up of animal model. Alb-
135 creERT2;*Glut9*$^{lox/lox}$ mice were injected intraperitoneally with tamoxifen and then fed an
136 acidogenic diet with inosine for 32 days. On day 14, HU+CU mice were injected with tofacitinib
137 or vehicle (control) every alternate day. (**B**) Serum IL-6 levels of tofacitinib- and vehicle-treated
138 HU+CU mice on day 32 (n = 5 mice per group). (**C** - **E**) Serum uric acid (**C**) and blood urea
139 nitrogen (BUN) levels (**D**), and glomerular filtration rate (GFR) (**E**) of tofacitinib- and vehicle-
140 treated HU+CU mice on day 14 and 32 (n = 5 mice per group, one- or two-way ANOVA). (**F**)
141 Representative images of periodic acid-Schiff (PAS, magnification: x200) staining illustrating
142 tubular injury in tofacitinib- and vehicle-treated HU+CU mice on day 32. (**G**) Intrarenal mRNA
143 expression levels of the kidney injury marker (*KIM-1*), interleukin 6 (*Il6*), tumor necrosis factor
144 (*Tnf*)*α*, inducible nitric oxide synthase (*iNos*), arginase 1 (*Arg1*) of tofacitinib- and vehicle-
145 treated HU+CU mice on day 32 (n = 5 mice per group, Student's t-test). (**H**) Representative
146 images of Picro sirius red staining illustrating interstitial fibrosis in tofacitinib- and vehicle-
147 treated HU+CU mice on day 32. Magnification: x200. (**I**) Intrarenal mRNA expression levels of
148 the fibrosis marker *Fibronectin 1* and collagen *(Col)1α1*. (**J** and **K**) Absolute number of kidney
149 M1-like macrophages (**J**, CD45^{+}MHCII^{+}F4/80^{hi}CD11b^{+}CD11c^{lo}CX3CR1^{+}CD206^{-}) and of M2-like
150 macrophages (**K**, CD45^{+}MHCII^{+}F4/80^{hi}CD11b^{+}CD11c^{lo}CX3CR1^{+}CD206^{+}) on day 32 determined
151 by flow cytometry (n = 5 mice per group, Student's t-test). (**L**) Number of crystal granulomas
152 on PAS-stained kidney sections (n = 5 mice per group, Student's t-test). Data are mean ± SD. *
153 p<0.05; ** p<0.01; *** p<0.001; ns, not significant.

154

155

156

157

158

159

160

3. Supplementary Movies

3.1 Supplementary Movie 1

3.2 Supplementary Movie 2 – move along z axis

180 **4. Supplementary Tables**

181 **4.1 Supplementary Table 1.** Murine primer sequences.

182

Mouse genes		Primer sequences
KIM-1	Forward	5‘-TCAGCTCGGGAATGCACAA-3‘
	Reverse	5‘-TGGTTGCCTTCCGTGTCTCT-3‘
Tnfα	Forward	5‘-CCACCACGCTCTTCTGTCTAC-3‘
	Reverse	5‘-AGGGTCTGGGCCATAGAACT-3‘
Il-6	Forward	5’-TGATGCACTTGCAGAAAACA-3’
	Reverse	5’-ACCAGAGGAAATTTTCAATAGGC-3’
iNos	Forward	5’-GAGACAGGGAAGTCTGAAGCAC-3’
	Reverse	5’-CCAGCAGTAGTTGCTCCTCTTC-3’
Arg1	Forward	5’-AGAGATTATCGGAGCGCCTT-3’
	Reverse	5’-TTTTTCCAGCAGACCAGCTT-3’
Col1α1	Forward	5‘-ACATGTTCAGCTTTGTGGACC-3‘
	Reverse	5‘-TAGGCCATTGTGTATGCAGC-3‘
Fibronectin 1	Forward	5‘-GGAGTGGCACTGTCAACCTC-3‘
	Reverse	5‘-ACTGGATGGGGTGGGAAT-3‘
FSP-1	Forward	5‘-CAGCACTTCCTCTCTCTTGG-3‘
	Reverse	5‘-TTTGTGGAAGGTGGACACAA-3‘
18s RNA	Forward	5‘-GCAATTATTCCCCATGAACG-3‘
	Reverse	5‘-AGGGCCTCACTAAACCATCC-3‘

183

184

185

186

187

188

189

190

191

192

193

194

195

196

197 5. **References**

198 1. Wilson, P.C. *et al.* The single-cell transcriptomic landscape of early human diabetic
199 nephropathy. *Proc Natl Acad Sci U S A* **116**, 19619-19625 (2019).
200 2. Butler, A., Hoffman, P., Smibert, P., Papalexi, E. & Satija, R. Integrating single-cell
201 transcriptomic data across different conditions, technologies, and species. *Nat Biotechnol* **36**,
202 411-420 (2018).
203 3. Edgar, R., Domrachev, M. & Lash, A.E. Gene Expression Omnibus: NCBI gene expression and
204 hybridization array data repository. *Nucleic Acids Res* **30**, 207-210 (2002).
205 4. Barrett, T. *et al.* NCBI GEO: archive for functional genomics data sets--update. *Nucleic Acids*
206 *Res* **41**, D991-995 (2013).
207 5. Neusser, M.A. *et al.* Human nephrosclerosis triggers a hypoxia-related glomerulopathy. *Am J*
208 *Pathol* **176**, 594-607 (2010).
209 6. Berthier, C.C. *et al.* Cross-species transcriptional network analysis defines shared
210 inflammatory responses in murine and human lupus nephritis. *J Immunol* **189**, 988-1001
211 (2012).
212 7. Ju, W. *et al.* Defining cell-type specificity at the transcriptional level in human disease.
213 *Genome Res* **23**, 1862-1873 (2013).
214 8. Martini, S. *et al.* Integrative biology identifies shared transcriptional networks in CKD. *J Am*
215 *Soc Nephrol* **25**, 2559-2572 (2014).
216 9. Hodgin, J.B. *et al.* The molecular phenotype of endocapillary proliferation: novel therapeutic
217 targets for IgA nephropathy. *PLoS One* **9**, e103413 (2014).
218 10. Tajti, F., Kuppe, C., Antoranz, A., Ibrahim, M.M., Kim, H., Ceccarelli, F., Holland, C.H., Olauson,
219 H., Floege, J., Alexopoulos, L.G., Kramann, R., Saez-Rodriguez, J. A functional landscape of
220 CKD entities from public transciptome data. *Kidney Int Rep* (2019).

221